ESR and Mössbauer Studies of Crystallization Process of Iron Phosphate Glass

Katsuhisa TANAKA, Naohiro SOGA,* Rikuo OTA, and Kazuyuki HIRAO
Department of Industrial Chemistry, Faculty of Engineering, Kyoto University, Yoshida, Sakyo-ku, Kyoto 606
(Received November 11, 1985)

$0.7Fe_2O_3$-$0.3P_2O_5$ glass was prepared by using a twin-roller method and the crystallization process of this glass was followed by means of ESR and Mössbauer spectroscopy in order to understand the state and the behavior of iron ions in the glass. The ESR line shape of the quenched $0.7Fe_2O_3$-$0.3P_2O_5$ glass was much broader than that of the crystallized glass heat-treated at 710 °C for 5 h. Moreover, the linewidth of Mössbauer spectra decreased monotonously through the crystallization process. These facts indicated that there existed a distribution of ligand fields around iron ions in the glass. The Mössbauer parameters, that is the isomer shift and the quadrupole splitting, of the $0.7Fe_2O_3$-$0.3P_2O_5$ glass showed that Fe^{3+} ions in this glass were laid on distorted octahedral ligand fields. The magnetic interaction working in the $0.7Fe_2O_3$-$0.3P_2O_5$ glass at room temperature was dipole-dipole interaction. Besides, the Mössbauer spectrum of the glass exhibited no internal field line at room temperature. Hence, the glass is considered paramagnetic at room temperature. At the first stage of crystallization process, the α-Fe_2O_3 particles precipitated were sufficiently small and so the specimen was superparamagnetic, as revealed from the ESR and Mössbauer spectra of heat-treated specimens.

Spin glass behavior of oxide glasses containing large amounts of iron(III) or iron(II) ions has attracted much attention recently as a number of attempts have been made to characterize their magnetic properties as well as the state of iron ions in these glasses. Although most of the studies carried out so far indicate that these glasses exhibit antiferromagnetic properties at low temperatures,[1-10] several papers[7-9] report that well below the freezing temperature, individual spins are frozen in random directions and a new magnetic phase, which shows speromagnetism,[11,12] appears. Thus, the magnetic structure of iron-containing oxide glass has not been completely clarified. More detailed informations about the state of iron ions in these glasses are needed to comprehend the characteristics of their magnetic properties. One approach is to use such a method as ESR or Mössbauer spectroscopy, which is sensitive to the local change around iron ions and to follow the change occurring during the crystallization process of iron-containing glasses.[13]

In the present work, Fe_2O_3–P_2O_5 binary glasses containing a much larger amount of iron oxide than that in the previously studied glasses were prepared by using a rapid quenching method. The choice of phosphate glass comes from the fact that P_2O_5 forms glass most easily with transition metal oxides. The ESR and Mössbauer spectra of these glasses were obtained to find out a glass structure having no trace of microcrystals. Then, the glass was subjected to heat treatment and the change in the state of iron ions was followed in detail by means of ESR and Mössbauer effect measurements in order to discuss the structure of glass containing a very large amount of iron oxide.

Experimental

The glass samples were prepared by using reagent-grade Fe_2O_3 and $FePO_4$ hydrate as starting materials. $FePO_4$ hydrate was kept in an electric furnace at 400 °C for several hours for the purpose of excluding water, and then it was mixed thoroughly with Fe_2O_3 in suitable proportions (Table 1) and sintered at 800—900 °C for 3 h in air. The resultant material was melted by heating it in an image furnace with a xenon lamp and the melt was rapidly quenched by falling it on a twin-roller rotating at 3000 rpm. The cooling rate of this method is about 10^5 K s^{-1}. The specimen obtained was a thin film of about 20 μm thickness. X-Ray diffraction measurements were employed to determine whether the specimen was amorphous or not.

Table 1. Compositions of Fe_2O_3–P_2O_5 Binary System and Results of X-Ray Diffraction Analysis

Composition/mol%		Results of X-ray diffraction
Fe_2O_3	P_2O_5	
50	50	Amorphous
60	40	Amorphous
70	30	Amorphous
75	25	Amorphous
76	24	Amorphous
77	23	Fe_3O_4 precipitated
80	20	Fe_3O_4 precipitated

For the heat treatment experiments, the $0.7Fe_2O_3$-$0.3P_2O_5$ glass was used. The heat treatment was carried out in an electric furnace at various temperatures from 220 to 710 °C for 5 h in air. The crystals precipitated in the heat treatment process were ascertained by X-ray diffraction analysis.

The ESR measurements were made using a JEOL PE-2X spectrometer operating at X-band frequency (ν=9.4 GHz) with 1.0×10^{-4} T magnetic modulation width at room temperature. Reference signals of Mn^{2+} ions in MgO were used as the standards for the linewidth and effective g-value.

The Mössbauer effect measurements were carried out at room temperature. As the γ-ray source, a 10 mCi ^{57}Co in metallic rhodium was used. The velocity calibration and the calculation of the isomer shift were made from the spectra of pure iron foil.

Results

Glass Forming Limit. The compositions of the specimens prepared to select a glass having no trace

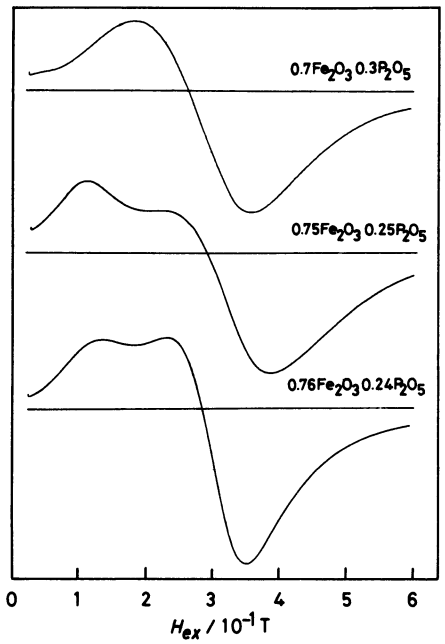

Fig. 1. ESR spectra of $0.7Fe_2O_3$–$0.3P_2O_5$, $0.75Fe_2O_3$–$0.25P_2O_5$, and $0.76Fe_2O_3$–$0.24P_2O_5$.

Table 2. ESR Linewidth and Effective g-Value of $0.7Fe_2O_3$–$0.3P_2O_5$, $0.75Fe_2O_3$–$0.25P_2O_5$, and $0.76Fe_2O_3$–$0.24P_2O_5$

Composition/mol%		ΔH	g_{eff}
Fe_2O_3	P_2O_5	10^{-1}T	
70	30	1.78	2.38
75	25	1.61	2.18
		0.46	4.29
76	24	1.23	2.18
		0.51	4.28

of microcrystals are summarized in Table 1 along with the results of X-ray diffraction analysis. The X-ray diffraction pattern of the specimen exhibited an amorphous state until the concentration of Fe_2O_3 reached up to 76 mol% and showed the appearance of Fe_3O_4 when the content of Fe_2O_3 exceeded 77 mol%. However, in the X-ray diffraction patterns of $0.75Fe_2O_3$–$0.25P_2O_5$ and $0.76Fe_2O_3$–$0.24P_2O_5$ one very weak peak was noticed in the halo pattern. The existence of a minute amount of some microcrystalline phase was confirmed by employing ESR and Mössbauer effect measurements on the three specimens, $0.7Fe_2O_3$–$0.3P_2O_5$, $0.75Fe_2O_3$–$0.25P_2O_5$, and $0.76Fe_2O_3$–$0.24P_2O_5$.

ESR spectra of these specimens are shown in Fig. 1. The linewidth and effective g-value obtained from these spectra are summarized in Table 2. As seen in Fig. 1, the spectra of $0.75Fe_2O_3$–$0.25P_2O_5$ and $0.76Fe_2O_3$–$0.24P_2O_5$ were different from that of $0.7Fe_2O_3$–$0.3P_2O_5$. The latter consisted of only one broad peak centered at g=2.0, but the former spectra were composed of two peaks at g=4.3 and 2.0. These peaks are attributable to the resonance of Fe^{3+} ion whose spin state is $^6S_{5/2}$.

Table 3. Results of Mössbauer Effect Measurements of $0.7Fe_2O_3$–$0.3P_2O_5$, $0.75Fe_2O_3$–$0.25P_2O_5$, and $0.76Fe_2O_3$–$0.24P_2O_5$

Composition/mol%		I.S.	Q.S.
Fe_2O_3	P_2O_5	mm s^{-1}	mm s^{-1}
70	30	Fe^{3+} 0.43	Fe^{3+} 1.18
		Fe^{2+} 1.06	Fe^{2+} 2.45
75	25	Fe^{3+} 0.41	Fe^{3+} 0.79
		Fe^{2+} 1.22	Fe^{2+} 2.41
76	24	Fe^{3+} 0.36	Fe^{3+} 0.78
		Fe^{2+} 1.10	Fe^{2+} 2.26

Table 4. Precipitated Crystals through the Crystallization Process of $0.7Fe_2O_3$–$0.3P_2O_5$ Glass

T_A [a]	t_A [a]	Results of X-ray diffraction
°C	h	
300	5	Amorphous
400	5	Amorphous
420	5	α-Fe_2O_3
500	5	α-Fe_2O_3, $Fe(PO_3)_2$
600	5	α-Fe_2O_3, $Fe(PO_3)_2$
710	5	α-Fe_2O_3, $FePO_4$, Fe_3PO_7

a) T_A and t_A mean heat treatment temperature and heat treatment time, respectively.

Table 3 shows the results of Mössbauer effect measurements. Fe^{2+} ions, which were not detectable in the ESR spectra, were detected in all the specimens. It is apparent from this table that the values of the quadrupole splitting of Fe^{3+} ions in both $0.75Fe_2O_3$–$0.25P_2O_5$ and $0.76Fe_2O_3$–$0.24P_2O_5$ are significantly smaller than that in $0.7Fe_2O_3$–$0.3P_2O_5$. This fact means that the symmetry of Fe^{3+} ion sites is more distorted in $0.7Fe_2O_3$–$0.3P_2O_5$ than in $0.75Fe_2O_3$–$0.25P_2O_5$ or $0.76Fe_2O_3$–$0.24P_2O_5$, because the quadrupole splitting is a measure of the symmetry of the environment around an iron ion. This result of Mössbauer effect measurements indicates the precipitation of some microcrystals in both $0.75Fe_2O_3$–$0.25P_2O_5$ and $0.76Fe_2O_3$–$0.24P_2O_5$, while no crystalline phase existed in the $0.7Fe_2O_3$–$0.3P_2O_5$ specimen. Thus, this composition was used for the following heat treatment experiments.

Change of ESR and Mössbauer Spectra upon Heat Treatment. The kinds of crystals, precipitated in the $0.7Fe_2O_3$–$0.3P_2O_5$ specimen during the crystallization process are summarized in Table 4. As seen in this table, α-Fe_2O_3 precipitated at 420 °C, and at 500 °C Fe^{2+} ions formed iron metaphosphate $Fe(PO_3)_2$.

Figure 2 shows the ESR spectra of the quenched $0.7Fe_2O_3$–$0.3P_2O_5$ glass and the specimen heat-treated at 710 °C. The former is apparently much broader than the latter.

The change in linewidth of ESR spectra appearing

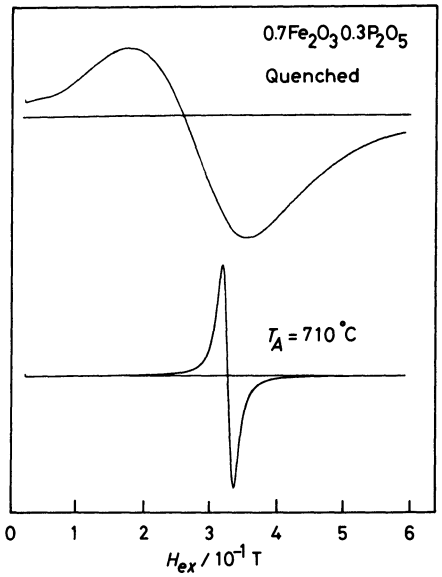

Fig. 2. ESR spectra of $0.7Fe_2O_3$-$0.3P_2O_5$ quenched glass and heat-treated at 710°C. T_A means the heat treatment temperature.

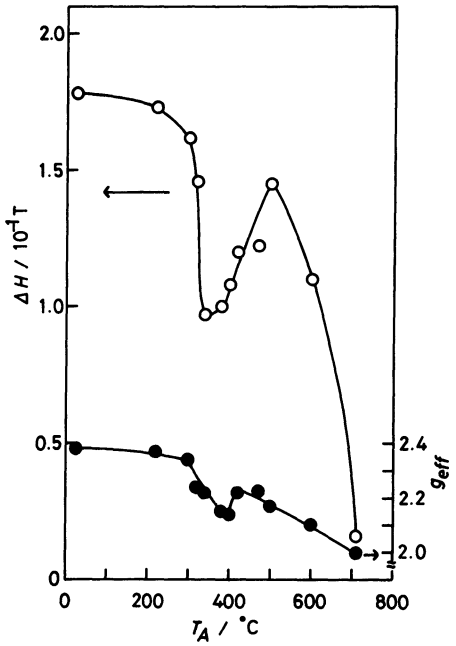

Fig. 3. Change on linewidth and effective g-value of ESR spectrum through the crystallization process of $0.7Fe_2O_3$-$0.3P_2O_5$ glass.

during the heat treatment process is shown in Fig. 3, along with the change of effective g-value. The linewidth started to decrease at about 300°C and took a minimum at about 340°C, beyond which it increased. When the heat treatment temperature exceeded 500°C, it decreased again rapidly. A similar tendency was seen on the change of effective g-value.

The change in linewidth of Mössbauer spectra appearing during the heat treatment process is shown in Fig. 4. The linewidth of Fe^{3+} did not change until

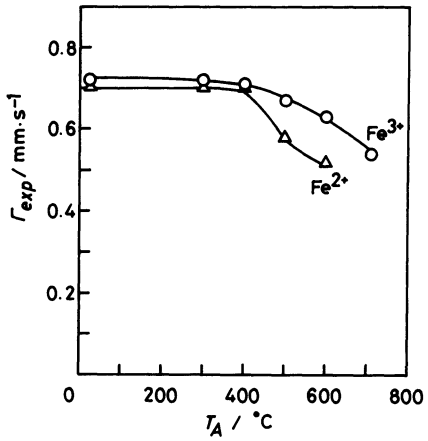

Fig. 4. Change on linewidth of Mössbauer spectra through the crystallization process.

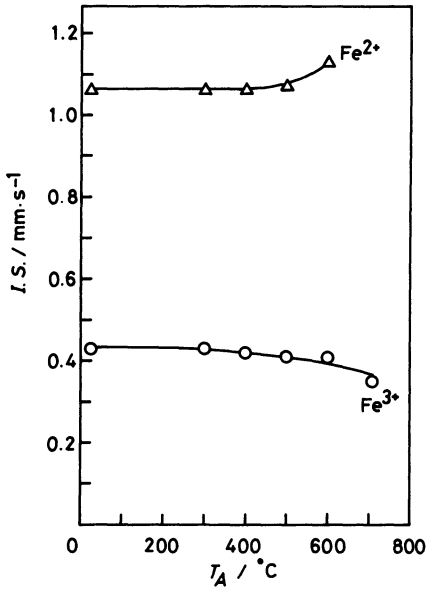

Fig. 5. Change on isomer shift of Fe^{3+} and Fe^{2+} through the crystallization process.

the heat treatment temperature reached up to 300°C and decreased monotonously when the heat treatment temperature exceeded 400°C, at which α-Fe_2O_3 microcrystals started to precipitate according to the X-ray diffraction measurements. The linewidth of Fe^{2+} also decreased at 400°C.

The change of isomer shift is shown in Fig. 5. The isomer shift of Fe^{3+} in the quenched $0.7Fe_2O_3$-$0.3P_2O_5$ glass was 0.43 mm s^{-1} when referred to pure iron. The isomer shift of Fe^{3+} decreased slowly through the crystallization process. On the contrary, the isomer shift of Fe^{2+} increased with increasing heat treatment temperature.

The change of quadrupole splitting, which is a measure of symmetry of the shape of electron clouds around an iron ion, is shown in Fig. 6. The quadrupole splitting of Fe^{2+} decreased at first and then increased as $Fe(PO_3)_2$ crystal grew. This change corresponds to

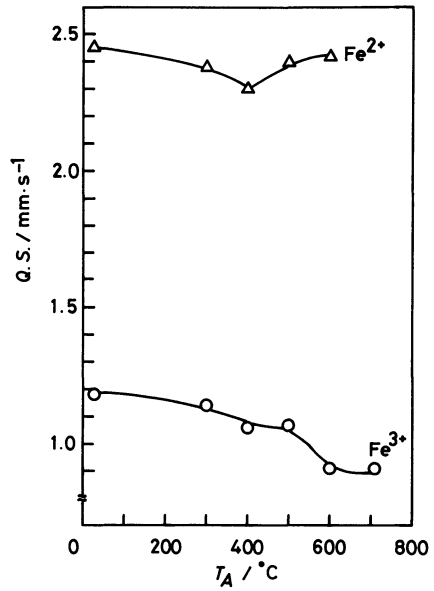

Fig. 6. Change on quadrupole splitting of Fe^{3+} and Fe^{2+} through the crystallization process.

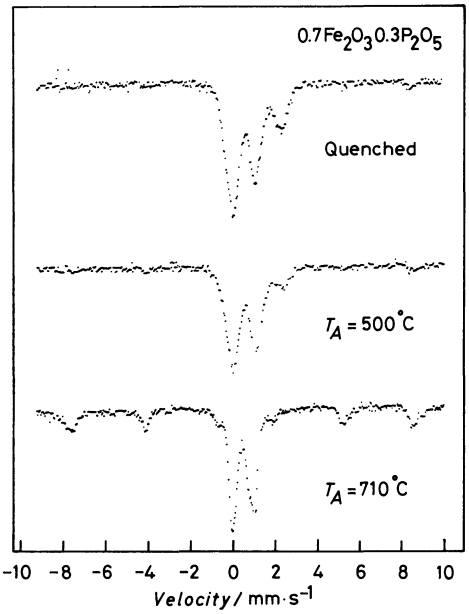

Fig. 7. Mössbauer spectra of quenched, heat-treated at 500°C, and heat-treated at 710°C, $0.7Fe_2O_3$–$0.3P_2O_5$ glass.

the change of isomer shift.

Discussion

ESR Spectra and Structural Change. The quenched glass showed much broader ESR spectra than the heat-treated specimen (Fig. 2). This fact indicates that the ligand field around Fe^{3+} fluctuates in $0.7Fe_2O_3$–$0.3P_2O_5$ glass. Generally, Hamiltonian yielding the energy levels of spin is written as follows:

$$H = g\beta HS + D\left\{S_z^2 - \frac{1}{3}S(S+1)\right\} + E(S_x^2 - S_y^2) + \frac{1}{6}a\left\{S_x^4 + S_y^4 + S_z^4 - \frac{1}{5}S(S+1)(3S^2+3S-1)\right\} + H_{ss} + H_{hf} + H_Q. \quad (1)$$

The first term is Zeeman energy and the second and the third terms are ligand field energies. The fourth term is fourth dimensional one of spin peculiar to Fe^{3+}, spin quantum number of which is larger than 2. H_{ss}, H_{hf}, and H_Q correspond to Hamiltonian representing spin-spin interaction, hyperfine interaction, and quadrupole interaction of nucleus, respectively. If there exists a variation of ligand fields, the crystal field parameters D and E are not uniform but fluctuate. So, Hamiltonian must be affected by the fluctuation, and the eigenvalue of Hamiltonian, that is the energy level of spin, should have a distribution. Therefore, the ESR spectrum of $0.7Fe_2O_3$–$0.3P_2O_5$ glass is expected to exhibit a very broad tail as observed in Fig. 2.

The linewidth of the quenched $0.7Fe_2O_3$–$0.3P_2O_5$ glass was 1.78×10^{-1} T, which is much larger than that of the specimen heat-treated at 710°C (1.60×10^{-2} T). The latter is attributable to the parasitic ferromagnetism of α-Fe_2O_3,[14,15] which causes a strong superexchange interaction at room temperature. According to the Anderson-Weiss theory,[16] the observed linewidth is represented as follows:

$$\Delta H = \frac{\frac{10}{3}(\Delta H_p)^2 + (\Delta H_H)^2}{\Delta H_e}, \quad (2)$$

where ΔH_p, ΔH_e, and ΔH_H represent the linewidth due to dipole–dipole interaction, exchange (superexchange) interaction, and fine structure field, respectively. Therefore, the linewidth of the specimen heat-treated at 710 °C should become very narrow due to the precipitation of α-Fe_2O_3. On the other hand, dipole–dipole interaction governs the magnetic interaction between iron ions in the quenched glass. Consequently, the linewidth of the quenched glass becomes broadened as indicated in Eq. 2.

A complicated change of linewidth with heat treatment temperature shown in Fig. 3 requires another mechanism of line narrowing than the superexchange interaction in the precipitated α-Fe_2O_3. According to Néel,[17] α-Fe_2O_3 is also known as a compound which shows superparamagnetism when the size of the particles is sufficiently small.

The smallness of the size of α-Fe_2O_3 precipitated in this temperature range can be demonstrated by the result of Mössbauer effect measurements. The Mössbauer spectrum of the specimen heat-treated at 500°C is drawn in Fig. 7 along with the spectra of the quenched glass as well as the specimen heat-treated at 710°C. Although α-Fe_2O_3 has already precipitated in

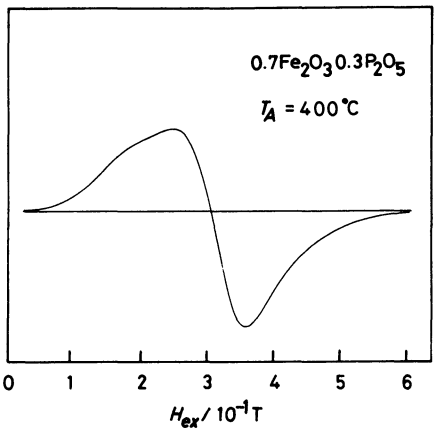

Fig. 8. ESR spectrum of $0.7Fe_2O_3$-$0.3P_2O_5$ glass heat-treated at 400°C.

the specimen heat-treated at 500°C as ascertained by X-ray diffraction analysis shown in Table 4, the sextet peak due to the internal field in α-Fe_2O_3 did not appear in this specimen. This fact indicates that α-Fe_2O_3 in this specimen is small and shows superparamagnetic. The existence of superparamagnetism can be seen in the ESR spectrum of the specimen heat-treated at 400°C shown in Fig. 8. The shoulder at about 1.8×10^{-1} T is attributable to Fe^{3+} ions which still exist in the glassy state in this specimen, and the peak at the higher field is due to Fe^{3+} ions in the superparamagnetic α-Fe_2O_3 particle. This ESR spectrum is very similar to that of ultrafine particles of Fe_3O_4 in various liquid observed by Sharma and Waldner.[18]

The line narrowing due to superparamagnetism was observed by Sharma and Waldner,[18] who investigated ultrafine particles of Fe_3O_4 in various ferrofluids by means of X-band ESR measurements. They defined the superparamagnetic narrowing factor f as follows:

$$f = \tau_{sp}/\tau_L = M_S V/\gamma k T \tau_L, \quad (3)$$

where τ_{sp} and τ_L are the superparamagnetic relaxation time and Larmor precession time, respectively, M_S is the saturation magnetization, V is the volume of the superparamagnetic particle, and γ is the gyromagnetic ratio. The proportional relation between the superparamagnetic narrowing linewidth and the volume of the particle was demonstrated by the data measured by Aharoni and Litt.[19] The increase in linewidth with increasing heat treatment temperature from 340 to 500°C observed in the present study is attributable to the growth of α-Fe_2O_3 crystallites.

When the heat treatment temperature exceeded 500°C, the linewidth decreased sharply. As described above, this narrowing is assigned to superexchange interaction owing to Fe^{3+} in α-Fe_2O_3 particles, the size of which is large enough not to show superparamagnetism. This interpretation agrees with the Mössbauer spectrum of the specimen heat-treated at 710°C in Fig. 7, which exhibited internal field lines. The internal field of α-Fe_2O_3 in this specimen is estimated to be 506 kOe ($1kOe=10^6/4\pi$ A m^{-1}).

As for the effective g-value, it was 2.00 for the specimen heat-treated at 710°C. This value is reasonable for Fe^{3+} ions because the spin state of Fe^{3+} is $^6S_{5/2}$ and its orbital angular momentum is zero. The effective g-value of the quenched $0.7Fe_2O_3$-$0.3P_2O_5$ glass was 2.38, larger than 2.00. This deviation from $g=2.00$ is ascribed to the contribution of orbital angular momentum to the g-value. The fraction of the orbital angular momentum in the total angular momentum, which is the sum of orbital angular momentum and spin angular momentum, is represented by the following relation:[20,21]

$$\varepsilon = \frac{1}{2}g - 1. \quad (4)$$

In the case of $0.7Fe_2O_3$-$0.3P_2O_5$ glass, $\varepsilon=0.19$. As described above, however, the orbital angular momentum quantum number of Fe^{3+} is zero, so that ε should be zero. The reason why ε was not zero in the $0.7Fe_2O_3$-$0.3P_2O_5$ glass is not clear at present, but might be related to the existence of Fe^{2+} ions in this glass. Fe^{2+} is known as an ion which is magnetically extremely anisotropic. The spin state of Fe^{2+} is $S=2$, $L=2$, indicating that the orbital angular momentum remains. In a general crystal such as an ionic crystal, this orbital angular momentum is quenched because of strong orbital-lattice interaction. Since there is a distribution of ligand field in this glass as described above, it is predictable that quenching of orbital angular momentum is not complete. Moreover, it may be presumed that there exists a resonance structure in this glass like the next one:

$$Fe^{2+}\text{-}O^{2-}\text{-}Fe^{3+} \rightleftarrows Fe^{3+}\text{-}O^{2-}\text{-}Fe^{2+}. \quad (5)$$

It is considered that Fe^{2+} has an effect on Fe^{3+} by way of such a resonance. As a result, the effective g-value becomes significantly larger than 2.00.

Mössbauer Parameters and State of Iron Ions. The linewidth of Mössbauer spectrum of $0.7Fe_2O_3$-$0.3P_2O_5$ glass was broader than that of the crystallized specimen (Fig. 4). This demonstrates a distribution of electric field gradient around both Fe^{3+} and Fe^{2+} ions in this glass. Eibschütz et al.[22] studied vitreous yttrium iron garnet by Mössbauer effect measurements and succeeded in fitting the computed absorption line to the experimental spectrum by assuming an asymmetric non-Gaussian distribution of electric field gradient. The existence of distribution of electric field gradient, that is a fluctuation of ligand field around Fe^{3+} ions, is ascertained by the shape of ESR spectra as described above.

The isomer shift of Fe^{3+} in the quenched $0.7Fe_2O_3$-$0.3P_2O_5$ glass (0.43 mm s^{-1}) shows that Fe^{3+} ions in this glass are coordinated by six O^{2-} ions as indi-

cated by Kurkjian and Sigety.[23] The change of isomer shift reflects the change in distance between an iron ion and an O^{2-} ion.[24] A smaller value of isomer shift shows a higher density of 4s-electrons around an iron ion, indicating the shorter distance between an iron ion and an O^{2-} ion. Therefore, the decrease of isomer shift of Fe^{3+} exhibits the decrease of the distance between Fe^{3+} and O^{2-} ions through the crystallization process and the increase of isomer shift of Fe^{2+} shows that the distance between Fe^{2+} and O^{2-} ions in $0.7Fe_2O_3$–$0.3P_2O_5$ glass is smaller than that in $Fe(PO_3)_2$ polycrystal.

The quadrupole splitting of Fe^{3+} directly reflects the geometrical symmetry of the coordination state of O^{2-} ions, because the 3d-orbitals of Fe^{3+} is half filled and the electric field gradient caused by 3d-electrons is tetrahedrally symmetrical. Hence, the decrease of quadrupole splitting of Fe^{3+} through the crystallization process reveals that the coordination state of O^{2-} ions around Fe^{3+} in $0.7Fe_2O_3$–$0.3P_2O_5$ glass is more asymmetrical than that in α-Fe_2O_3.

The increase of isomer shift of Fe^{2+} after $Fe(PO_3)_2$ precipitated may be explained by the decrease of 4s-electron density of Fe^{2+} as described above. Because of the decrease of 4s-electron density, the nucleus of iron in Fe^{2+} interacts more easily with 3d-electrons. Since five 3d-orbitals of Fe^{2+} is filled with six electrons, the electric field gradient induced by 3d-electrons of Fe^{2+} is significantly asymmetrical. So, the quadrupole splitting of Fe^{2+} increases with decreasing 4s-electron density as $Fe(PO_3)_2$ crystals grow.

Structure of $0.7Fe_2O_3$–$0.3P_2O_5$ Glass. The structure and magnetic properties of $0.44Fe_2O_3$–$0.56P_2O_5$ glass were investigated by Egami et al.[2] using susceptibility measurements and neutron diffraction analysis, and by Wedgwood and Wright[3] using neutron diffraction analysis. Although Egami et al. suggested that it is microcrystalline, Wedgwood and Wright gave a different interpretation and proposed that the glass is composed of two phases, one of which is a silica-like network containing alternate FeO_4 and PO_4 tetrahedra and another is chains of PO_4.

For $0.7Fe_2O_3$–$0.3P_2O_5$ glass studied in the present paper, the glass structure of a silica-like network composed of alternate FeO_4 and PO_4 tetrahedra is not suitable, because the coordination number of O^{2-} ion around Fe^{3+} is 6 as shown by the Mössbauer effect measurements. The glass consists of FeO_6 octahedra instead of FeO_4 tetrahedra.

Furthermore, no microcrystalline phase was detected in the present $0.7Fe_2O_3$–$0.3P_2O_5$ glass. As shown by the broader line shape of ESR spectrum and the broader linewidth of Mössbauer spectrum for $0.7Fe_2O_3$–$0.3P_2O_5$ glass, there is a distribution of ligand fields around iron ions in the glass. Moreover, the coordination state around iron ions in the glass is more unsymmetrical than that in the precipitated crystal. These facts show that $0.7Fe_2O_3$–$0.3P_2O_5$ glass is not microcrystalline but has a disordered state.

Besides, the magnetic interaction between iron ions working in $0.7Fe_2O_3$–$0.3P_2O_5$ glass at room temperature was dipole-dipole interaction, indicating that this glass is paramagnetic at room temperature. This fact also ruled out the existence of microcrystals in this glass. If microcrystals were to exist and the glass were superparamagnetic at room temperature, the superparamagnetic line of ESR spectrum would have been detected in this glass and its linewidth would have been narrow as observed at the first stage of precipitation of α-Fe_2O_3 in the crystallization process.

At the present moment it is considered that $0.7Fe_2O_3$–$0.3P_2O_5$ glass contains an assemblage of Fe^{3+} and Fe^{2+} which definitely has a magnetic anisotropy. Although it is still uncertain whether such assemblage is possible in a completely random state or not, it seems easier to make a resonance structure of Fe^{3+} and Fe^{2+} from a slightly disordered state, or *pseudo*-microcrystal or *quasi*-microcrystal structure (like monodomains proposed by Verhelst et al.[25]), which fluctuates a little in the glass.

The authors express their great thanks to Dr. Yasuhito Isozumi at the Kyoto University Radioisotope Research Center for the Mössbauer effect measurements and his kind advice on the discussion.

References

1) A. W. Simpson and J. M. Lucas, *J. Appl. Phys.*, **42**, 2181 (1971).
2) T. Egami, O. A. Sacli, A. W. Simpson, A. L. Terry, and F. A. Wedgwood, *J. Phys. C: Solid State Phys.*, **5**, L261 (1972).
3) F. A. Wedgwood and A. C. Wright, *J. Non-Cryst. Solids*, **21**, 95 (1976).
4) E. J. Friebele, L. K. Wilson, A. W. Dozier, and D. L. Kinser, *Phys. Status. Solidi B*, **45**, 323 (1971).
5) E. M. Gyorgy, K. Nassau, M. Eibschütz, J. V. Waszczak, C. A. Wang, and J. C. Shelton, *J. Appl. Phys.*, **50**, 2883 (1979).
6) H. Laville and J. C. Bernier, *J. Mater. Sci.*, **15**, 73 (1980).
7) O. Horie, Y. Syono, Y. Nakagawa, A. Ito, K. Okamura, and S. Yajima, *Solid State Commun.*, **25**, 423 (1978).
8) Y. Syono, A. Ito, and O. Horie, *J. Phys. Soc. Jpn.*, **46**, 493 (1979).
9) J. P. Sanchez, J. M. Friedt, R. Horne, and A. J. van Duyneveldt, *J. Phys. C: Solid State Phys.*, **17**, 127 (1984).
10) S. K. Mendiratta, R. Horne, and A. J. van Duyneveldt, *Solid State Commun.*, **52**, 371 (1984).
11) J. M. D. Coey, *J. Phys. (Paris), Colloq.*, **35**, C6-89 (1974).
12) J. M. D. Coey, *J. Appl. Phys.*, **49**, 1646 (1978).
13) T. Komatsu and N. Soga, *J. Chem. Phys.*, **72**, 1781 (1980).
14) I. Dzyaloshinsky, *J. Phys. Chem. Solids*, **4**, 241 (1958).
15) T. Moriya, *Phys. Rev. Lett.*, **4**, 228 (1960).
16) P. W. Anderson and P. R. Weiss, *Rev. Mod. Phys.*, **25**, 269 (1953).

17) L. Néel, *Rev. Mod. Phys.*, **25**, 293 (1953).
18) V. K. Sharma and F. Waldner, *J. Appl. Phys.*, **48**, 4298 (1977).
19) S. M. Aharoni and M. H. Litt, *J. Appl. Phys.*, **42**, 352 (1971).
20) C. Kittel, *Phys. Rev.*, **76**, 743 (1946).
21) J. H. Van Vleck, *Phys. Rev.*, **78**, 266 (1950).
22) M. Eibschütz, M. E. Lines, and K. Nassau, *Phys. Rev. B*, **21**, 3767 (1980).
23) C. R. Kurkjian and E. A. Sigety, *Phys. Chem. Glasses*, **9**, 73 (1968).
24) T. Komatsu and N. Soga, *J. Appl. Phys.*, **51**, 601 (1980).
25) R. A. Verhelst, R. W. Kline, A. M. de Graaf, and H. O. Hooper, *Phys. Rev. B*, **11**, 4427 (1975).